



# Low magnitude high frequency vibrations expedite the osteogenesis of bone marrow stem cells on paper based 3D scaffolds

Ozge Karadas<sup>1</sup> · Gulistan Mese<sup>2</sup> · Engin Ozcivici<sup>1</sup>

Received: 21 March 2020 / Revised: 12 June 2020 / Accepted: 27 June 2020 / Published online: 6 July 2020  
© Korean Society of Medical and Biological Engineering 2020

## Abstract

Anabolic effects of low magnitude high frequency (LMHF) vibrations on bone tissue were consistently shown in the literature *in vivo*, however *in vitro* efforts to elucidate underlying mechanisms are generally limited to 2D cell culture studies. Three dimensional cell culture platforms better mimic the natural microenvironment and biological processes usually differ in 3D compared to 2D culture. In this study, we used laboratory grade filter paper as a scaffold material for studying the effects of LMHF vibrations on osteogenesis of bone marrow mesenchymal stem cells in a 3D system. LMHF vibrations were applied 15 min/day at 0.1 g acceleration and 90 Hz frequency for 21 days to residing cells under quiescent and osteogenic conditions. mRNA expression analysis was performed for alkaline phosphatase (ALP) and osteocalcin (OCN) genes, Alizarin red S staining was performed for mineral nodule formation and infrared spectroscopy was performed for determination of extracellular matrix composition. The highest osteocalcin expression, mineral nodule formation and the phosphate bands arising from the inorganic phase was observed for the cells incubated in osteogenic induction medium with vibration. Our results showed that filter paper can be used as a model scaffold system for studying the effects of mechanical loads on cells, and LMHF vibrations induced the osteogenic differentiation of stem cells.

**Keywords** Vibration · Filter paper · Mesenchymal stem cells · Scaffold · Osteogenic differentiation

## 1 Introduction

Bone tissue is dynamically remodeled throughout an organism's lifespan to meet mechanical demand with proper morphological adaptations [1] and to remove accumulating micro defects [2]. This process is very well integrated to the fracture healing phases, resulting in a scar tissue free regenerative process [3]. However, some insults on the bone tissue that occur as a result of trauma, surgery or diseases such as osteonecrosis might cause critical sized defects that cannot be repaired without surgical procedures [4], signifying a need for functional bone substitutes. Though it is possible to augment critical sized defects using biomaterial based grafts [5], mechanical mismatch, poor biodegradability of many natural polymers, low cell attachment, acidic byproduct

formation and alterations in mechanical properties of synthetic polymers upon degradation limits applicability of biomaterials [6]. Alternatively, bone tissue engineering aims to produce functional bone substitutes *ex vivo* by mimicking natural bone environment with scaffolds, autologous cells and relevant biochemical or physical signals [7].

For bone tissue engineering applications, scaffolds are needed to provide the structure for cells to invade and populate. Various natural and synthetic materials are shown to be suitable as scaffolds for the bone tissue [8, 9]. Cellulose is one of these natural materials, which can be extracted from various organisms from plants to bacteria and can be used as a scaffold material because of its abundance, low cost, tunable mechanical properties and surface chemistry [10]. Paper is an industrialized product of cellulose and a wide range of paper types with different physical and mechanical properties are commercially available to be used for technological applications. Laboratory grade filter paper (Whatman) is an example of pure cellulose product that does not contain any additional binders in its structure [11]. Recent biotechnological applications of the paper use include the production of disposable high throughput analytical test systems,

✉ Engin Ozcivici  
enginozcivici@iyte.edu.tr

<sup>1</sup> Department of Bioengineering, Rm A210, Izmir Institute of Technology, Urla, Izmir 35430, Turkey

<sup>2</sup> Department of Molecular Biology and Genetics, Izmir Institute of Technology, Urla, Izmir, Turkey

biosensors, electronic devices, cell and tissue culture platforms because of its biocompatibility, ease of modifications, low cost and availability [12–16]. Furthermore, filter paper is shown to be a promising scaffold material for tissue engineering because of its formability which makes it possible to produce centimeter scale scaffolds by folding [11].

Another important component of a tissue engineered construct is the cell. For bone tissue, osteoblasts and osteocytes are responsible for the bone modeling and remodeling, so osteoblasts and precursor cells are considered as the primary cell sources for bone repair studies [17]. Stem cells, on the other hand, are capable of proliferation for a long time in vitro and differentiation into different lineages upon stimulation. Bone marrow mesenchymal stem cells (BM MSCs) are the most abundantly utilized stem cell source because of their high osteogenic potential [18]. The last components for tissue engineering, the biochemical or physical signals, are required to mimic the in vivo microenvironment. Various mechanical loads are exerted on all tissues in human body; such as the compression on bones and cartilages, tension on muscles and tendons, fluid shear in blood vessels and hydrodynamic pressure in the heart valves [19]. Structural and functional adaptations occur in bone tissue upon application of mechanical forces. Adaptation of skeletal tissue to mechanical loads depends heavily on genetic and epigenetic factors [20–27]. Besides biological factors, the physical properties of the mechanical loads also influence the subsequent skeletal adaptations. Anabolic effects of mechanical forces on bone tissue are based on several parameters such as the magnitude [28], frequency [28–31], rate, cycle number [32] and distribution of the mechanical loads [33]. When applied within the physiological range, dynamic mechanical loading triggers in vivo bone formation in contrary to continuous static loading, which might cause tissue resorption [34, 35].

Many different tools to induce mechanotransduction events have been used up to now, such as micropipette aspiration, fluid shear and hydrostatic pressure, but vibrations are utilized as mechanical stimulators lately as an alternative [36]. Low magnitude loads (usually < 1 g acceleration) with high frequencies (20–90 Hz) are commonly referred as vibrations and application of vibrations have anabolic effects on bone [31, 37–40]. Even though the magnitude of the mechanical loads differ depending on the daily activities and physical exercise, the bones are subjected to a continuous low magnitude high frequency force arising from muscle action in the resting state [34], which can be imitated through the use of vibrational forces [41].

The effects of vibrational forces are usually studied for monolayer cells and there is limited research about their application on 3D in vitro culture systems. In this research, we utilized vibrational forces as a stimulator for osteogenic differentiation of mouse bone marrow mesenchymal stem

cells on filter paper-based scaffolds and differentiation of the cells was determined by gene expression analysis, mineral staining and infrared spectroscopy. To our knowledge, this report is the first description of paper-based tissue engineering scaffolds to be used for 3D in vitro mechanotransduction studies and our results indicate that these scaffolds are suitable candidates to be used for bone tissue engineering applications.

## 2 Materials and methods

### 2.1 Cell culture and osteogenic induction

D1 ORL UVA (mouse bone marrow) cell line was infected with EGFP (enhanced green fluorescent protein) and Puromycin resistance gene carrying retroviruses in order to produce fluorescently labelled stable cell lines. EGFP gene was transferred by pMIG viral vector (Addgene #9044, USA). For infection D1 ORL UVA cells were first seeded at a density of  $3 \times 10^4$  cells/cm<sup>2</sup>. Growth media of the cells (DMEM high glucose with 10% FBS and 1% Pen/Strep) were replaced with infection medium ((virus suspension in growth medium with Polybrene (1:1000 v/v)) on the next day after cell seeding. Normal growth medium with Polybrene and without the virus was used as the negative control. The next day, infection medium was replaced with normal growth medium and cells were incubated in this medium for 2 days. Infected cells were selected with Puromycin (2 µg/mL) containing medium (DMEM high glucose with 10% FBS and 1% Pen/Strep). EGFP carrying D1 ORL UVA (D1 ORL UVA-EGFP) cells were seeded on circular filter paper (Whatman® Grade 114, 190 µm thickness and 25 µm average pore size, Merck, Germany) constructs at a density of  $10^2$  or  $10^4$  cells in 20 µL directly in 12 well plates or on filter papers [42]. For osteogenic induction, on the next day of cell seeding the regular growth medium of cells was replaced with osteogenic induction medium (10 mM β-glycerophosphate, 50 µg/mL ascorbic acid and DMEM high glucose with 10% FBS and 1% Pen/Strep).

### 2.2 Application of low magnitude high frequency (LMHF) signals

D1 ORL UVA-EGFP cells seeded in 12 well plates and on filter paper scaffolds were exposed to LMHF vibrations daily at 90 Hz and 0.1 g (1 g = Earth's gravitational pull), for 15 min/day, 5 days/week at ambient conditions for 21 days. LMHF was generated and delivered to cells by a custom-made platform in vertical direction (Fig. 1), similar to our previous studies on monolayer cultures [43, 44].

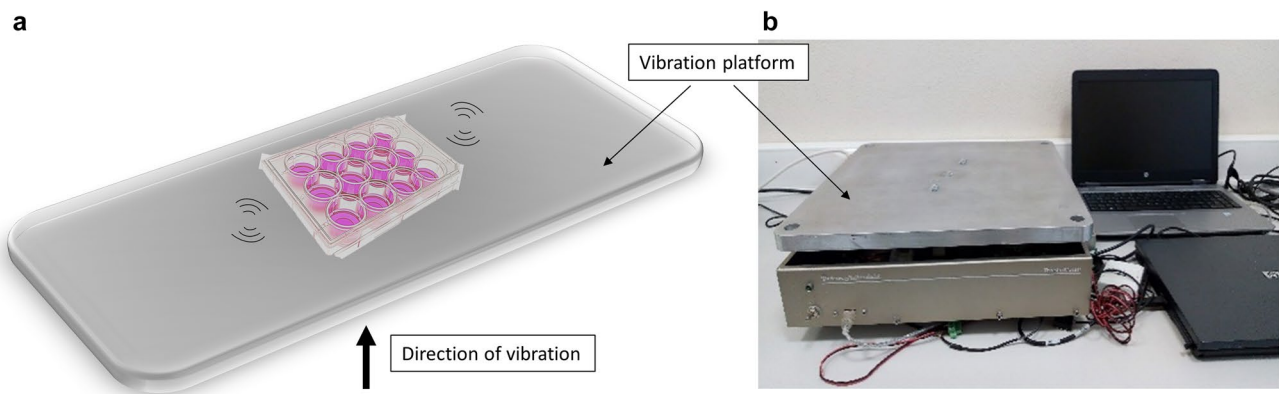


**Fig. 1** The schematic representation **a** and photography **b** of the vibration platform utilized in the study

### 2.3 Determination of cell viability on Whatman paper

The effect of LMHF on the viability of cells was determined by MTT assay on days 1, 3, 7 and 10 after seeding. Regular growth media of the samples were replaced by 10% MTT solution containing medium, incubated for 4 h at 37 °C and 5% CO<sub>2</sub>. Tetrazolium salts were solubilized with DMSO and the absorbance was measured at 570 and 650 nm wavelengths with a spectrophotometer (Thermo Fisher Scientific, Multiscan Spectrum, USA). Empty filter paper that was incubated with the same amount of MTT containing medium for the same duration was used as blank and its absorbance value was subtracted from absorbance values collected from experimental samples.

### 2.4 Total RNA isolation from paper scaffolds and RT-PCR

Total RNA isolation was done from D1 ORL UVA cells (passage no < 20) that were seeded on filter paper scaffolds at a density of 10<sup>5</sup> cells/paper on the 14th day of incubation. PureLink RNA Mini Kit (Invitrogen, USA) was used for RNA isolation. Paper samples were washed with PBS once and then transferred into separate microcentrifuge tubes. The samples were homogenized with a tissue grinder within the lysis buffer (Isolab, Germany). The cells were suspended

by passing the suspension through insulin needles several times and then 70% ethanol was added to each sample and RNA purification was done according to the manufacturer's instructions. The concentration and purity of isolated RNAs were measured by NanoDrop spectrophotometer.

Reverse transcription was done by using RevertAid First Strand cDNA Synthesis Kit (ThermoFisher Scientific, USA), according to the manufacturer's instructions with 220 ng template RNA. For RT-PCR 55 ng cDNA was used with the primers listed below. PCR was conducted at 95 °C for 30 s, 60 °C for 30 s and 72 °C for 30 s for 45 cycles. The annealing temperatures are given in (Table 1). Quantitative RT-PCR was done by Light Cycler 96 thermal cycler (Roche, Switzerland) with FastStart Essential DNA Green Master Kit (Roche, Switzerland).

The relative expression levels of the target genes were calculated by threshold cycle ( $\Delta\Delta C_t$ ) method with GAPDH as a reference gene and reported as  $2^{-\Delta\Delta C_t}$ , as relative fold-changes to samples under static and growth medium conditions.

### 2.5 Determination of mineralization in tissue culture plates and on filter paper scaffolds

Cell seeded filter paper constructs and tissue culture plates were washed with 10 mM PBS and fixed with 4% paraformaldehyde (PFA) (Sigma-Aldrich, USA). Alizarin red

**Table 1** Forward and reverse primers used for RT-qPCR reactions

Gene	Forward primer (5'–3')	Reverse primer (5'–3')	Annealing temperature (°C)
OCN	CTG ACA AAG CCT TCA TGT CCA A	GCG CCG GAG TCT GTT CAC TA	55.9
ALP	TTT AGT ACT GGC CAT CGG CA	ATT GCC CTG AGT GGT GTT GCA	57.9
GAPDH	GAC ATG CCG CCT GGA GAA AC	AGC CCA GGA TGC CCT TTA GT	58

S (ARS) dye solution (2% w/v) was prepared and samples were stained with ARS dye, by incubating them at 37 °C for 30 min. Then the samples in tissue culture plates were washed with distilled water. For the cells on filter paper scaffolds, a blank empty paper was used as a reference to understand whether the non-specifically bound dye was removed or not. Additional rinsing was done by adding PBS and leaving the samples on a shaker overnight. The following day samples were washed with distilled water by leaving them in water for a total of 3 h on the shaker and renewing the water at every hour. After aspiration of the water, the samples were stored at –20 °C before extraction of the dye with Cetylpyridinium Chloride (CPC) [45]. For extraction, CPC solution with 10% (w/v) concentration in 10 mM sodium phosphate (pH 7.0) was prepared. ARS stained samples were incubated in CPC solution in a 24 well plate for 1 h at room temperature on a shaker. 100 µL aliquots from each sample was transferred as triplicate to a 96-well plate and the absorbance was measured at 550 nm. ARS concentration per sample was calculated and the values were normalized to total protein amount.

### 2.5.1 Total protein isolation and determination of the amount from cells on paper scaffolds

Lysis buffer (10 mM Tris-HCl pH=7.5, 1 mM EDTA, 0.1% Triton X, protease inhibitor 1% (v/v) and dithiothreitol (DTT, 0.1% v/v)) was prepared. Tissue culture plates and paper scaffolds with cells were washed with PBS. Tissue culture plates were put on ice directly and paper samples were transferred to microcentrifuge tubes in ice. Complete lysis buffer was added to each sample and the samples were vortexed 10 s with 5 min intervals during a total of 30 min. Lysates were centrifuged at 15000 rpm for 3 min and supernatants were transferred to fresh tubes. Total protein contents were measured by Bradford assay. Bradford reagent (20%, v/v) was diluted with distilled water (80%, v/v). Diluted Bradford reagent was aliquoted in separate microcentrifuge tubes and 10% (v/v) isolated protein was added to tubes, and 100 µL from each sample was transferred to a 96-well plate as triplicate and the absorbance was read at 595 nm.

### 2.5.2 FTIR analyses for detection of mineralization

The composition of organic and inorganic components of ECM was detected by Fourier-transform infrared spectroscopy (FTIR) (Perkin Elmer Spectrum Version 10.4.3, USA). The samples were fixed with 4% PFA and washed with distilled water. Water has a strong infrared absorbance [46], thus samples were dried in the vacuum oven to remove water prior to FTIR analysis. FTIR spectrometer with ATR attachment was used and the spectra were recorded in the range of 4000–400 cm<sup>-1</sup> wavenumber with 4 cm<sup>-1</sup> resolution. FTIR

spectra of the samples were compared with empty paper that was treated with the same procedures for cell fixation and washing steps. Since the fingerprint peaks of bone originating from collagen and hydroxyapatite are within 400–1700 cm<sup>-1</sup> region of the spectrum, the comparison between spectra of different samples was done by narrowing the wavenumber interval. Analyses were done by using Spectragryph 1.2 spectroscopy software.

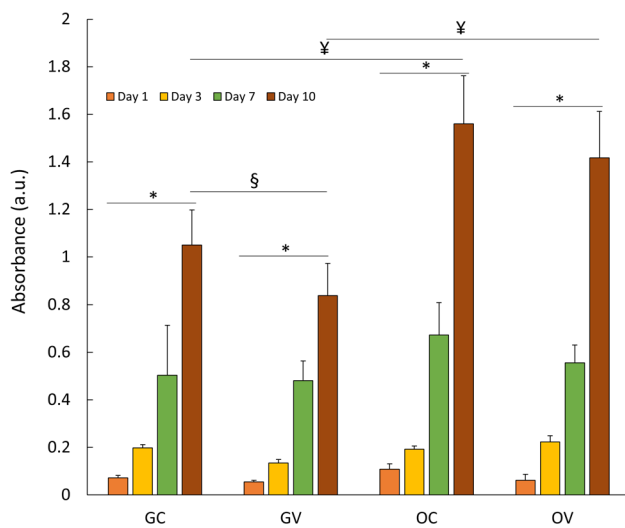
## 2.6 Statistical analyses

All the experiments were repeated in triplicates, and all results are displayed as the mean ± standard deviation. Statistical analyses for comparison between the groups were performed using ANOVA. In order to detect significant difference in growth, Student's t-test was performed between control and vibration groups of each condition. To demonstrate the differences between groups for gene expression and quantification of mineralization ANOVA followed by S-N-K post hoc test was done. Levels of significance were reported for 5%, 1%, and 0.1%.

## 3 Results

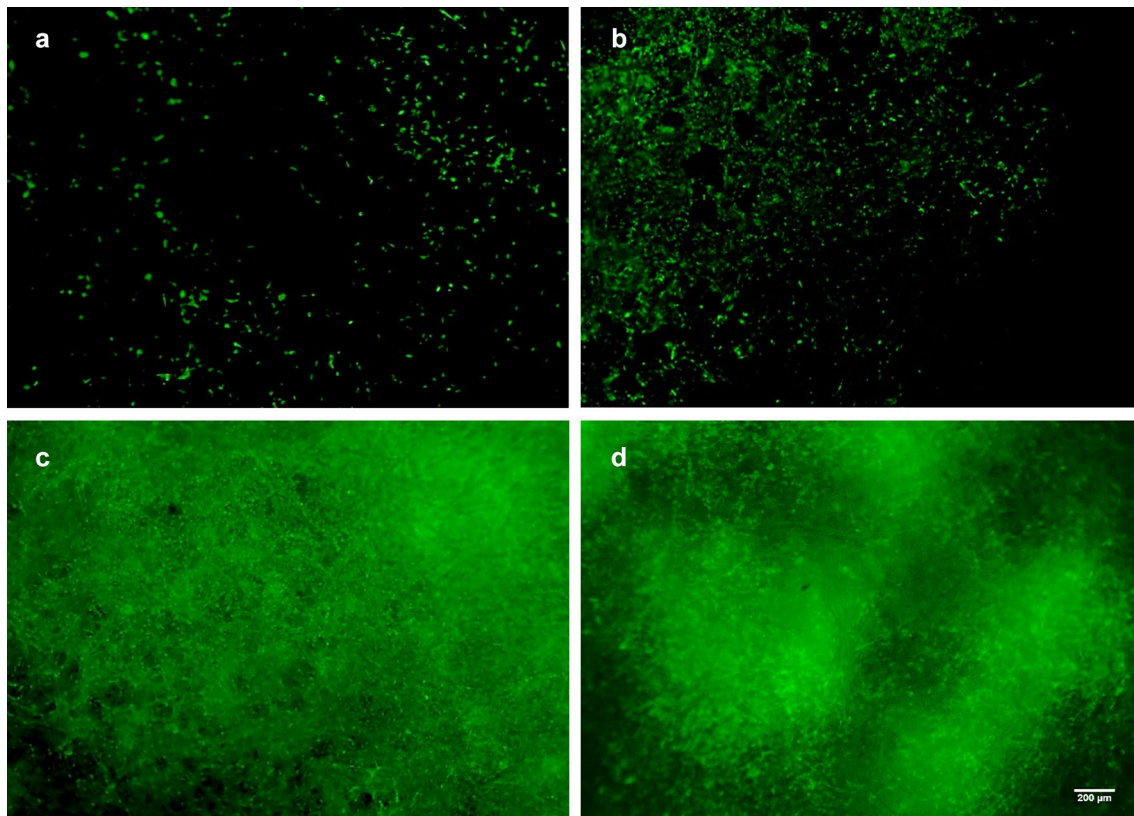
The viability of D1 ORL UVA stem cells on filter paper scaffolds was determined via MTT assay for both standard growth and osteogenic induction conditions with or without exposure to vibration. The viability signal on paper scaffolds increased during 10 days for all conditions (Fig. 2), and at day 10, growth control (GC), growth vibration (GV), osteogenic control (OC) and osteogenic vibration (OV) cells had 14.7-fold, 14.8-fold, 14.5-fold and 23.5-fold (all  $p < 0.001$ ) increase compared to the day 1 signal of corresponding group, respectively. At day 10, daily vibrations showed effect on the MTT signal of cells cultured on growth conditions (–23%,  $p < 0.05$ ), but not for osteogenic conditions. On the other hand, presence of osteogenic conditions induced 49% and 79% (both  $p < 0.001$ ) increase in MTT signals for control and vibrated cells at day 10, respectively. Continued proliferation and viability of D1 ORL UVA cells were validated on paper based scaffolds for 3 weeks via fluorescent signals for cells that were kept in growth conditions (Fig. 3).

In order to determine the effect of osteogenic conditions and the vibrational loading on the osteogenic differentiation of D1 ORL UVA mesenchymal stem cells, Alizarin red S (ARS) staining on the 14th day was assessed for GC, GV, OC and OV groups for cells cultured on 2D plates (Fig. 4). As expected, mineral formation was not evident for GC and GV groups, but OC and OV groups were stained densely on the 14th day of incubation (Fig. 4a). Quantification of ARS staining by CPC extraction demonstrated that OV group deposited



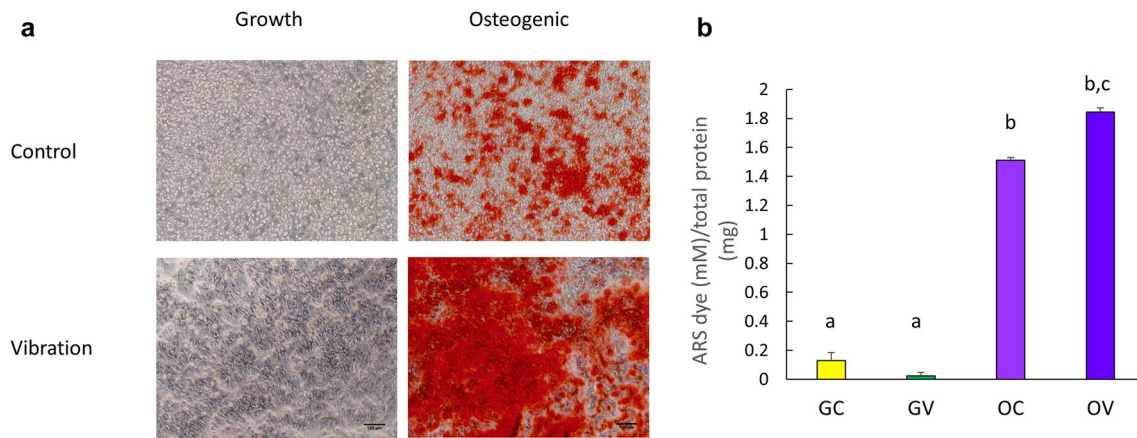
**Fig. 2** The viability of D1 ORL UVA cells on filter paper scaffolds was determined via MTT assay. Cell viability was assessed under normal growth and osteogenic induction conditions for 10 days. \*:  $p \leq 0.05$  between day 1 and day 10; §:  $p \leq 0.05$  between control and vibration at day 10; ¥:  $p \leq 0.05$  between growth and osteogenic condition at day 10; calculated by ANOVA followed by S-N-K post-hoc test. *GC* growth control, *GV*: growth vibration, *OC*: osteogenic control, *OV* osteogenic vibration

15, 92 and 1.3-fold more calcium than GC, GV and OC groups ( $p < 0.001$  for all), respectively (Fig. 4b). Subsequently, mineral formation was tested for D1 ORL UVA cells on 3D paper scaffolds (Fig. 5). Similar to 2D conditions, calcium deposition was only observed under osteogenic treatment condition on both the 14th and 21st days (Fig. 5a). The density of the extracted dye was almost 2-fold higher on day 21 compared to day 14 within both OC ( $p < 0.01$ ) and OV ( $p < 0.05$ ) groups (Fig. 5b). Similar to 2D culture results, calcium deposition in OV group was 1.5- and 1.4-fold higher than OC group for 14th ( $p < 0.001$ ) and 21st ( $p < 0.05$ ) days, respectively. Molecular indicators of osteogenesis were also tested at the 14th day of culture on paper scaffolds by semi-quantitative RT-PCR using the housekeeping gene GAPDH and further normalized to GC group (Fig. 6). Osteogenic medium treatment on D1 ORL UVA cells without the application of vibration caused 1.8-fold increase in OCN expression. The OCN expression of OV was 2.8 and 1.5-fold higher than GC ( $p < 0.001$ ) and OC ( $p < 0.01$ ), respectively. Induction of osteogenesis decreased ALP expression of OC and OV 2.7- and 2.9-fold, respectively compared to GC ( $p < 0.01$ ) at 14th day and daily exposure to LMHF



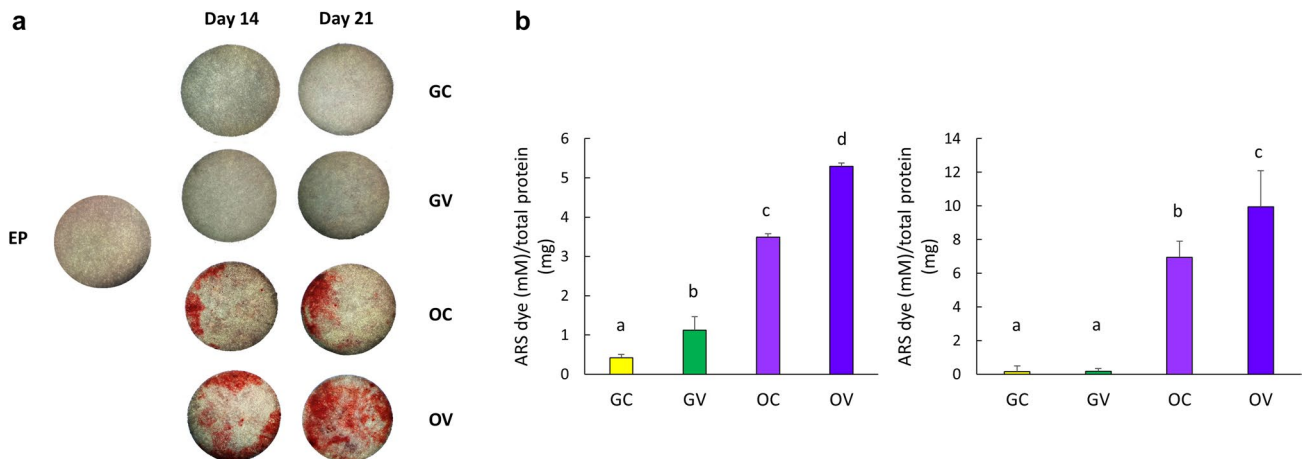
**Fig. 3** Fluorescent microscope images of D1 ORL UVA-EGFP cells showing proliferation of cells on filter paper scaffolds; **a** day 1, **b** day 7, **c** day 14 and **d** day 21 after cell seeding. Scale bar: 200  $\mu\text{m}$ . *GC*

growth control, *GV* growth vibration, *OC* osteogenic control and *OV* osteogenic vibration



**Fig. 4** **a** Phase contrast micrographs of D1 ORL UVA cells in tissue culture plates, stained with Alizarin red on day 14. Scale bar: 100  $\mu$ m. Red color indicates calcium deposits. **b** Quantification of Alizarin red S (ARS) staining by CPC extraction normalized to total protein.

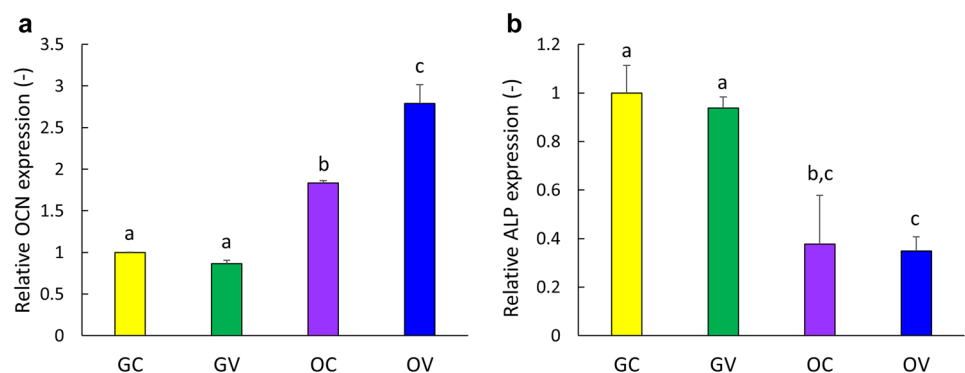
**a–c** Differences in dissolved ARS dye concentration between groups calculated by ANOVA followed by S-N-K post hoc test for  $p \leq 0.05$ . GC growth control, GV growth vibration, OC osteogenic control, OV osteogenic vibration



**Fig. 5** **a** Stereomicroscope images of D1 ORL UVA cells seeded on paper scaffolds, incubated in regular growth medium or osteogenic induction medium and stained with Alizarin red on days 14 and 21. Red color indicates calcium deposits. **b** Quantification of Alizarin red S (ARS) staining by CPC extraction normalized to total protein. a,

b, c: differences in dissolved ARS dye concentration between groups calculated by ANOVA followed by S-N-K post hoc test for  $p \leq 0.05$ . GC growth control, GV growth vibration, OC osteogenic control, OV osteogenic vibration, EP empty paper

**Fig. 6** Gene expression levels of D1 ORL UVA stem cells that were induced either with application of vibration or with osteogenic induction medium treatment after 14 days. a, b, c: differences in gene expression level between groups calculated by ANOVA followed by S-N-K post hoc test for  $p \leq 0.05$ . GC growth control, OC osteogenic control, GV growth vibration, OV osteogenic vibration



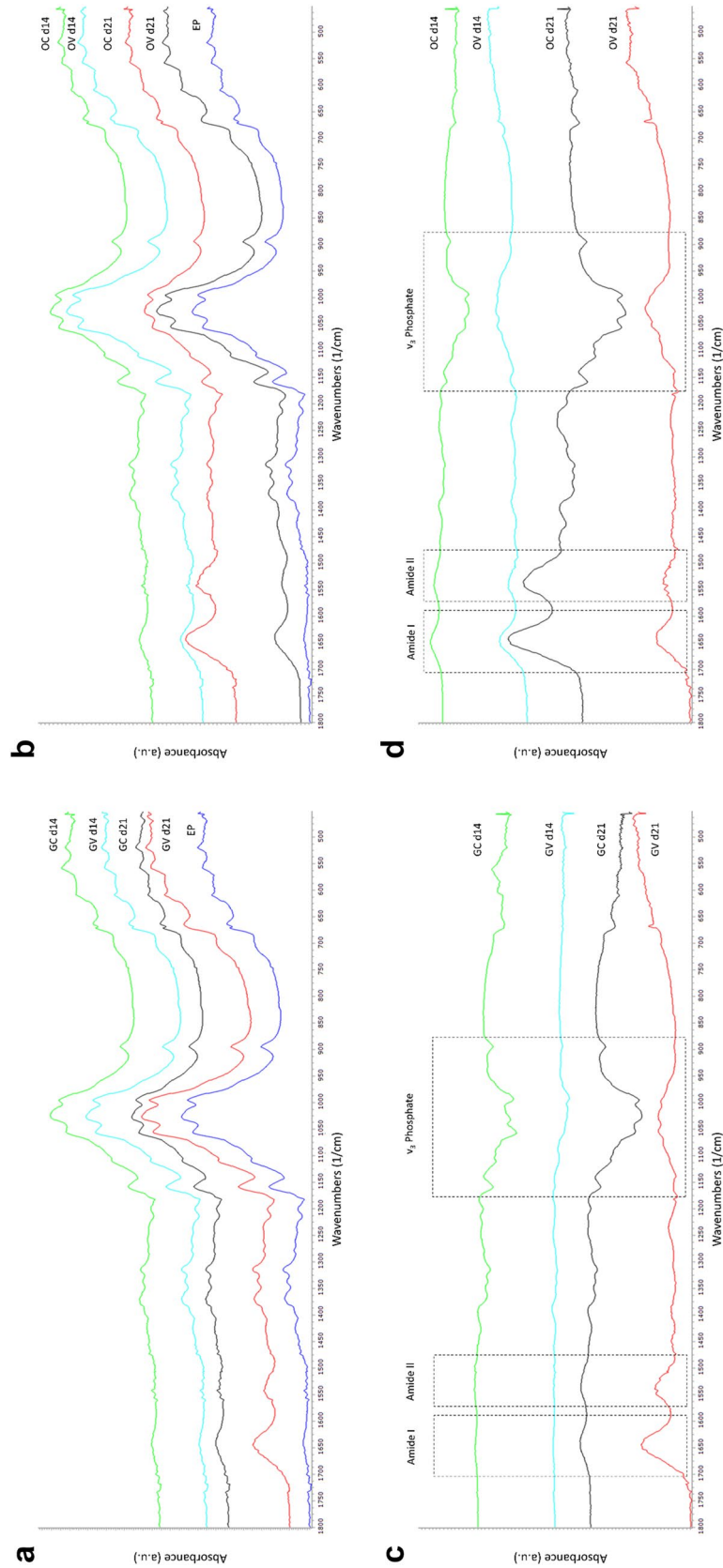


**Fig. 7** FTIR spectra of filter paper samples with D1 ORL UVA stem cells that were incubated in regular growth media or osteogenic media for 14 and 21 days with vibration or under static conditions. **a** Spectra of samples incubated in growth medium and the non-cell seeded empty paper, **b** spectra of samples incubated in osteogenic induction medium and empty paper **c** spectra of samples in growth condition after the spectrum of empty paper was subtracted from each and **d** spectra of samples in osteogenic condition after the spectrum of empty paper was subtracted from each. *GC* growth control, *GV* growth vibration, *OC* osteogenic control, *OV* osteogenic vibration, *EP* empty paper, *d14*: 14th day of cell culture, *d21*: 21st day of cell culture

vibrations did not further affect ALP levels of D1 ORL UVA cells.

To determine the extracellular matrix (ECM) composition generated by D1 ORL UVA cells cultured on paper based scaffolds, FTIR spectra of the specimens that were incubated in regular growth medium (Fig. 7a) and in osteogenic induction medium (Fig. 7b) were obtained. ECM composition of the samples at each condition was further analyzed by subtracting the spectrum of non-cell seeded empty paper (EP) from each sample spectrum on the 14th and 21st days of culture for both the samples in growth medium (Fig. 7c) and in osteogenic induction medium (Fig. 7d). It was observed that both GV and OV samples had peaks in Amide I and Amide II regions, as well as peaks in  $\nu_3$  phosphate region after 21 days of incubation (Fig. 7c, d), indicating the production of collagen and mineral phases. At the 14th day, OV group (Fig. 7d), but not the GV group (Fig. 7c), had both amide and phosphate peaks, indicating that ECM formation and mineralization. OC group, on the other hand, had peaks only in Amide I and II regions without a phosphate peak after 21 days of cell culture (Fig. 7d).

## 4 Discussion

Mechanical loading of cells with low magnitude high frequency vibrations in 2D cell culture and translational *in vivo* studies were frequently studied [38, 47–50], however research on the application of vibrational forces for 3D *in vitro* systems in the literature is extremely limited [51]. The aim of this study was to design a 3D *in vitro* model system for studying the effects of mechanical signals on osteogenesis. According to our results, low magnitude high frequency vibrations applied for 15 min/day triggered the osteogenic differentiation of stem cells on paper scaffolds more than chemical osteogenic induction alone, which was determined by gene expression analyses, ECM formation and mineralization.

It was previously reported that the application of vibrations on cells cultured in 3D *in vitro* cell culture systems, especially scaffolds derived from natural polymers, might not be suitable for understanding the isolated effects of vibrations because of the scaffold's promoting effect on osteogenesis [52]. However, in our research, osteogenic differentiation was not observed for the non-vibrated cells on scaffolds without chemical inducers suggesting that paper scaffolds can be used as model systems for studying the effects of vibrational forces in 3D cell cultures.

During osteogenic differentiation of stem cells, expression of osteoblast specific markers and mineralization related genes such as osteocalcin (OCN), osteopontin (OPN), osteonectin and bone sialoprotein (BSP) is upregulated [53].

OCN secretion might not be at a detectable level in the medium at the proliferation phase, but its expression rate is elevated with progression of nodule formation and reaches the maximum level after initiation of nodule mineralization [54]. According to our RT-PCR results, the highest amount of OCN expression was observed in OV group. This result demonstrates that application of vibrational forces induced osteogenic differentiation of MSCs on filter paper scaffolds more than the cells incubated under static conditions in osteogenic induction media. In a previous research that was performed by our research group, it was demonstrated that the effect of vibration on the expression of OCN gene was not significant in a 2D cell culture system [43]. However, in the present research, the vibrational forces with the same magnitude and frequency stimulated a significant increase in the expression of OCN gene for the same D1 ORL UVA bone marrow stem cells on 3D paper scaffolds compared to static conditions. Contrarily, a decrease in the ALP gene expression was observed upon incubation of the constructs with osteogenic induction medium on the 14th day. ALP is an early and transient marker of osteogenesis and after the mineral nodules start to form, ALP expression decreases over time [55]. Our results were also in consistence with the previous reports showing a decrease in the ALP gene expression in long term osteogenic induced samples that were stained positively for mineral deposition, suggesting that D1 ORL UVA stem cells were successfully differentiated into mineral forming osteoblasts on paper-based scaffolds.

Mineralization of the ECM initiates with the binding of calcium and phosphate ions to charged amino acid residues of collagen matrix [56–58]. Various forms of calcium phosphate crystals such as amorphous calcium phosphate, octacalcium phosphate,  $\beta$ -tricalcium phosphate and dicalcium phosphate dehydrate can be found in the medium during the formation and maturation of the hydroxyapatite (HAP) crystals in the ECM [57, 59–61]. ARS dye stains calcium and all types of calcium phosphates [62, 63] and it binds approximately 2 moles of  $\text{Ca}^{2+}$  per mole of dye in solution [64]. According to the FTIR scanning results of the samples, peaks arising from phosphate moieties were not observed for OC group, which was stained positively for deposited calcium. Before maturation of HAP crystals, the initial amorphous calcium phosphate precipitates formed can also be detected with ARS staining. Detection of mineral formation by ARS staining, but not through FTIR scanning might be a result of immature calcium phosphate deposits that could not be determined through phosphate stretching in HAP region through FTIR. In addition to that, OCN is a calcium binding protein and it is responsible for the nucleation and propagation of HAP crystal formation [65]. It was previously shown that knock-down of OCN gene causes a delay in the maturation of HAP crystals [57]. The higher OCN expression, the denser ARS staining and phosphate peaks obtained via FTIR scanning for



OV group samples in our study indicate that the application of vibrational forces triggered the formation of more mature mineral crystals than non-vibrated group.

The infrared spectrum of bone consists of bands both from native hydroxyapatite (at 500–700  $\text{cm}^{-1}$  and 900–1200  $\text{cm}^{-1}$ ) and collagen (at 1200–1700  $\text{cm}^{-1}$ ) because of its composite structure [66]. It also contains a band around 870  $\text{cm}^{-1}$  which is characteristic to type B apatite and arises from carbonate moieties [66]. FTIR data lead to important information on composition including mineral to matrix ratio, the mineral and collagen maturity and crystallinity [67]. The changes in the secondary structure of collagen also give information about the maturity of ECM which can be detected around 1650 (Amide I) and 1550 (Amide II) wavenumbers ( $\text{cm}^{-1}$ ) [67]. Important information can be gathered from infrared spectroscopy scans of the mineral phase obtained from homogenized in vitro cultures about the localization of ions with asymmetric vibrations [68]. As an example, mineral phase deposition was characterized by FTIR in a research about the potential use of Runx 2 expressing dermal fibroblast cells for bone tissue engineering applications, and Amide I/II bands at 1655 and 1550  $\text{cm}^{-1}$ , together with an enhanced phosphate peak at 1100  $\text{cm}^{-1}$  were reported for the cells that have osteogenic capacity [69]. Furthermore, the composition of bone nodules formed by BMSCs on chitosan/PMMA scaffolds was analyzed by FTIR and compared to murine calvariae and it was reported that the structure of tissue engineered nodules was almost identical to the mineral phase obtained from the mice [70]. Similarly, the in vitro mineralized ECM of MC3T3-E1 cells had absorption bands at 1200–900  $\text{cm}^{-1}$  range arising from phosphate group of the mineral in the ECM and amide I/II/III bands at 1650–1635  $\text{cm}^{-1}$ , 1550–1535  $\text{cm}^{-1}$  and 1240  $\text{cm}^{-1}$ , respectively [71]. In our research, characterization of the chemical composition of ECM formed by MSCs via FTIR demonstrated that the formation of phosphate peak from mineral phase and amide I/II peaks from the organic component collagen was triggered upon application of vibration for 21 days even without chemical inducers in the culture media. The peaks in the amide regions demonstrated that chemical osteogenic induction for both 14 and 21 days caused collagen deposition in the ECM, but the application of vibration together with osteogenic induction triggered mineral deposition in addition to protein. However, phosphate peak was not observed in the FTIR scans of the samples incubated for a shorter duration (14 days), which shows that vibration alone was not enough for mineral formation. Amide and phosphate bands was only observed for the samples that were incubated in osteogenic induction media and stimulated with vibrational forces for shorter incubation duration. Our results show that in order to form a mature mineralized ECM, cells should be stimulated by both chemical and mechanical induction. Aside from the presence of the amide and phosphate bands,

the lack of carbonate bands in our samples that were cultured in osteogenic conditions might be the result of shorter incubation durations and due to this, less mature hydroxyapatite formation compared to similar studies in the literature [69].

Briefly, the results obtained from this study demonstrated the importance of the application of mechanical forces for the stimulation of in vitro osteogenic differentiation as well as the use of a 3D cell culture platform. Additionally, our study confirmed the suitability of the filter paper as a scaffold material for studying the effects of mechanical loads on in vitro differentiation. Paper-based scaffolds can further be used as model systems to mimic the 3D structure of especially cancellous bone and these scaffolds can serve as important platforms for 3D bone-related mechanotransduction studies. Besides, the foldable nature of paper allows flexibility for constructing scaffolds with different geometries. Finally, standard size and porosity, as well as low cost, make paper scaffolds desirable candidates for bone tissue engineering studies. Our study, in this instance, describes that a 3D standardized study is possible for low magnitude vibrations for bone tissue engineering applications. The proposed scaffold systems have the potential to be translated especially for non-load bearing bone defect applications such as the facial bones because of the mechanical mismatch between bone and paper. However, paper allows a certain degree of compression through folding, suggesting that its mechanical properties can be further attenuated for load-bearing bones as well.

**Acknowledgements** Financial support from The Scientific and Technological Research Council of Turkey (215S862—EO) and Turkish Academy of Sciences (Young Investigator Award—EO) is gratefully acknowledged. We are thankful for the helpful discussions with Ozden Yalcin-Ozuyisal, PhD. The Izmir Institute of Technology, Biotechnology and Bioengineering Research Center is also appreciated for instrumental support.

## Compliance with ethical standards

**Conflict of interest** The authors declare that they have no conflict of interests.

**Ethical approval** This article does not contain any studies with animals performed by any of the authors.

## References

1. Hadjidakis DJ, Androulakis II, Bone remodeling. *Ann N Y Acad Sci.* 2006;1092:385–96.
2. Boyce BF, Rosenberg E, de Papp AE, Duong LT. The osteoclast, bone remodelling and treatment of metabolic bone disease. *Eur J Clin Invest.* 2012;42(12):1332–41.

3. Marsell R, Einhorn TA. The biology of fracture healing. *Injury*. 2011;42(6):551–5.
4. Schemitsch EH. Size matters: defining critical in bone defect size! *J Orthop Trauma*. 2017;31(Suppl 5):S20–2.
5. Sheikh Z, Hamdan N, Ikeda Y, Grynypas M, Ganss B, Glogauer M. Natural graft tissues and synthetic biomaterials for periodontal and alveolar bone reconstructive applications: a review. *Biomater Res*. 2017;21:9–9.
6. Haugen HJ, Lyngstadaas SP, Rossi F, Perale G. Bone grafts: which is the ideal biomaterial? *J Clin Periodontol*. 2019;46(S21):92–102.
7. Dang M, Saunders L, Niu X, Fan Y, Ma PX. Biomimetic delivery of signals for bone tissue engineering. *Bone Research*. 2018;6(1):25.
8. Qu H, Fu H, Han Z, Sun Y. Biomaterials for bone tissue engineering scaffolds: a review. *RSC Advances*. 2019;9(45):26252–62.
9. Chocholata P, Kulda V, Babuska V. Fabrication of scaffolds for bone-tissue regeneration. *Materials (Basel)*. 2019;12(4):568.
10. Courtenay JC, Sharma RI, Scott JL. Recent Advances in Modified Cellulose for Tissue Culture Applications. *Molecules*. 2018;23(3):654.
11. Camci-Unal G, Laromaine A, Hong E, Derda R, Whitesides GM. Biomineralization guided by paper templates. *Sci Rep*. 2016;6:1–12.
12. Ng K, Gao B, Yong KW, Li Y, Shi M, Zhao X, Li Z, Zhang X, Pingguan-Murphy B, Yang H, Xu F. Paper-based cell culture platform and its emerging biomedical applications. *Mater Today*. 2017;20(1):32–44.
13. Deiss F, Mazzeo A, Hong E, Ingber DE, Derda R, Whitesides GM. Platform for high-throughput testing of the effect of soluble compounds on 3D cell cultures. *Anal Chem*. 2013;85(17):8085–94.
14. Mosadegh B, Dabiri BE, Lockett MR, Derda R, Campbell P, Parker KK, Whitesides GM. Three-dimensional paper-based model for cardiac ischemia. *Adv Healthc Mater*. 2014;3(7):1036–43.
15. Camci-Unal G, Newsome D, Eustace BK, Whitesides GM. Fibroblasts enhance migration of human lung cancer cells in a paper-based coculture system. *Adv Healthc Mater*. 2016;5(6):641–7.
16. Kim S-H, Lee HR, Yu SJ, Han M-E, Lee DY, Kim SY, Ahn H-J, Han M-J, Lee T-I, Kim T-S, Kwon SK, Im SG, Hwang NS. Hydrogel-laden paper scaffold system for origami-based tissue engineering. *Proc Natl Acad Sci USA*. 2015;112(50):15426–31.
17. Marolt D, Knezevic M, Novakovic GV. Bone tissue engineering with human stem cells. *Stem Cell Res Ther*. 2010;1(2):10.
18. Orciani M, Fini M, Di Primio R, Mattioli-Belmonte M. Biofabrication and bone tissue regeneration: cell source, approaches, and challenges. *Front Bioeng Biotechnol*. 2017;5:17–7.
19. Su F-C, Wu C-C, Chien S. Roles of microenvironment and mechanical forces in cell and tissue remodeling. *J Med Biol Eng*. 2011;31:233–44.
20. Steiniche T, Eriksen EF. Chap. 15—Age-related changes in bone remodeling. In: Orwoll ES, editor. *Osteoporosis in men*. San Diego: Academic Press; 1999. p. 299–312.
21. Demontiero O, Vidal C, Duque G. Aging and bone loss: new insights for the clinician. *Ther Adv Musculoskelet Dis*. 2012;4(2):61–76.
22. Zhou B, Wang J, Stein EM, Zhang Z, Nishiyama KK, Zhang CA, Nickolas TL, Shane E, Guo XE. Bone density, microarchitecture and stiffness in Caucasian and Caribbean Hispanic postmenopausal American women. *Bone Res*. 2014;2:14016.
23. Razi H, Birkhold AI, Weinkamer R, Duda GN, Willie BM, Checa S. Aging leads to a dysregulation in mechanically driven bone formation and resorption. *J Bone Miner Res*. 2015;30(10):1864–73.
24. Boskey AL, Coleman R. Aging and bone. *J Dent Res*. 2010;89(12):1333–48.
25. Judex S, Zhang W, Donahue LR, Ozcivici E. Genetic loci that control the loss and regain of trabecular bone during unloading and reambulation. *J Bone Miner Res*. 2013;28(7):1537–49.
26. Ozcivici E, Zhang W, Donahue LR, Judex S. Quantitative trait loci that modulate trabecular bone's risk of failure during unloading and reloading. *Bone*. 2014;64:25–32.
27. Ozcivici E, Judex S. Trabecular bone recovers from mechanical unloading primarily by restoring its mechanical function rather than its morphology. *Bone*. 2014;67:122–9.
28. Ozcivici E, Kim Luu Y, Adler B, Qin Y-X, Rubin J, Judex S, Rubin C. Mechanical signals as anabolic agent in bone. *Nat Rev Rheumatol*. 2010;6:50–9.
29. Hsieh YF, Turner CH. Effects of loading frequency on mechanically induced bone formation. *J Bone Miner Res*. 2001;16(5):918–24.
30. Beck BR, Kent K, Holloway L, Marcus R. Novel, high-frequency, low-strain mechanical loading for premenopausal women with low bone mass: early findings. *J Bone Miner Metab*. 2006;24(6):505–7.
31. Olcum M, Baskan O, Karadas O, Ozcivici E. Application of low intensity mechanical vibrations for bone tissue maintenance and regeneration. *Turk J Biol*. 2016;40(2):300–7.
32. Srinivasan S, Weimer DA, Agans SC, Bain SD, Gross TS. Low-magnitude mechanical loading becomes osteogenic when rest is inserted between each load cycle. *J Bone Miner Res*. 2002;17(9):1613–20.
33. Rubin J, Rubin C, Jacobs CR. Molecular pathways mediating mechanical signaling in bone. *Gene*. 2006;367:1–16.
34. Thompson WR, Yen SS, Rubin J. Vibration therapy: clinical applications in bone. *Curr Opin Endocrinol Diabetes Obes*. 2014;21(6):447–53.
35. Stoltz JF, Dumas D, Wang X, Payan E, Mainard D, Paulus F, Maurice G, Netter P, Muller S. Influence of mechanical forces on cells and tissues. *Biorheology*. 2000;37(1–2):3–14.
36. Shikata T, Shiraishi T, Tanaka K, Morishita S, Takeuchi R. Effects of acceleration amplitude and frequency of mechanical vibration on osteoblast-like cells. 2007.
37. Judex S, Rubin CT. Is bone formation induced by high-frequency mechanical signals modulated by muscle activity? *J Musculoskel Neuronal Interact*. 2010;10(1):3–11.
38. Lau E, Al-Dujaili S, Guenther A, Liu D, Wang L, You L. Effect of low-magnitude, high-frequency vibration on osteocytes in the regulation of osteoclasts. *Bone*. 2010;46(6):1508–15.
39. Ozcivici E, Garman R, Judex S. High-frequency oscillatory motions enhance the simulated mechanical properties of non-weight bearing trabecular bone. *J Biomech*. 2007;40(15):3404–11.
40. Ozcivici E, Luu YK, Rubin CT, Judex S. Low-level vibrations retain bone Marrow's osteogenic potential and augment recovery of trabecular bone during reambulation. *PLoS ONE*. 2010;5(6):e11178.
41. Edwards JH, Reilly GC. Vibration stimuli and the differentiation of musculoskeletal progenitor cells: Review of results in vitro and in vivo. *World J Stem Cells*. 2015;7(3):568–82.
42. Karadas O, Mese G, Ozcivici E. Cytotoxic tolerance of healthy and cancerous bone cells to anti-microbial phenolic compounds depend on culture conditions. *Appl Biochem Biotechnol*. 2019;188(2):514–26.
43. Demiray L. Bone marrow stem cells adapt to low-magnitude vibrations by altering their cytoskeleton during quiescence and osteogenesis Turkish. *J Biol*. 2015;39:88–97.
44. Baskan O, Mese G, Ozcivici E. Low-intensity vibrations normalize adipogenesis-induced morphological and molecular changes of adult mesenchymal stem cells. *Proc Inst Mech Eng H*. 2017;231(2):160–8.
45. Gregory CA, Gunn WG, Peister A, Prockop DJ. An Alizarin red-based assay of mineralization by adherent cells in culture:

- comparison with cetylpyridinium chloride extraction. *Anal Biochem.* 2004;329(1):77–84.
46. Boskey A, Pleshko Camacho N. FT-IR imaging of native and tissue-engineered bone and cartilage. *Biomaterials.* 2007;28(15):2465–78.
  47. Zhou Y, Guan X, Liu T, Wang X, Yu M, Yang G, Wang H. Whole body vibration improves osseointegration by up-regulating osteoblastic activity but down-regulating osteoblast-mediated osteoclastogenesis via ERK1/2 pathway. *Bone.* 2015;71:17–24.
  48. Halonen HT, Hyttinen JAK, Ihalainen TO, Mechanical impact stimulation platform tailored for high-resolution light microscopy. *Health Technol;* 2019.
  49. Edwards JH, Reilly GC. Vibration stimuli and the differentiation of musculoskeletal progenitor cells: review of results in vitro and in vivo. *World J Stem Cells.* 2015;7(3):568.
  50. Benjakul S, Jitpukdeebodindra S, Leethanakul C. Effects of low magnitude high frequency mechanical vibration combined with compressive force on human periodontal ligament cells in vitro. *Eur J Orthod.* 2017;40(4):356–63.
  51. Baskan O, Karadas O, Mese G, Ozcivici E. Applicability of low-intensity vibrations as a regulatory factor on stem and progenitor cell populations. *Curr Stem Cell Res Therapy.* 2020;15(5):391–9.
  52. Mehta S, McClarren B, Ajiz A, Chalaby R, Cook-Chennault K, Olabisi RM. The effect of low-magnitude, high-frequency vibration on poly(ethylene glycol)-microencapsulated mesenchymal stem cells. *J Tissue Eng.* 2018;9:2041731418800101.
  53. Hanna H, Mir LM, Andre FM. In vitro osteoblastic differentiation of mesenchymal stem cells generates cell layers with distinct properties. *Stem Cell Res Ther.* 2018;9(1):203–3.
  54. Collin P, Nefussi JR, Wetterwald A, Nicolas V, Boy-Lefevre ML, Fleisch H, Forest N. Expression of collagen, osteocalcin, and bone alkaline phosphatase in a mineralizing rat osteoblastic cell culture. *Calcif Tissue Int.* 1992;50(2):175–83.
  55. Golub E, Boesze-Battaglia K. The role of alkaline phosphatase in mineralization. *Curr Opin Orthop.* 2007;18:444–8.
  56. Landis WJ, Jacquet R. Association of calcium and phosphate ions with collagen in the mineralization of vertebrate tissues. *Calcif Tissue Int.* 2013;93(4):329–37.
  57. Tsao Y-T, Huang Y-J, Wu H-H, Liu Y-A, Liu Y-S, Lee OK. Osteocalcin mediates biomineralization during osteogenic maturation in human mesenchymal stromal cells. *Int J Mol Sci.* 2017;18(1):159.
  58. An J, Leeuwenburgh S, Wolke J, Jansen J. 4—Mineralization processes in hard tissue: bone. In: Aparicio C, Ginebra M-P, editors. *Biomineralization and biomaterials.* Boston: Woodhead Publishing; 2016. p. 129–46.
  59. Boskey AL. Mineral-matrix interactions in bone and cartilage. *Clin Orthop Relat Res.* 1992;281:244–74.
  60. Johnsson MS, Nancollas GH. The role of brushite and octacalcium phosphate in apatite formation. *Critical reviews in oral biology medicine: an official publication of the American Association of Oral Biologists.* 1992;3(1–2):61–82.
  61. Xie B, Halter TJ, Borah BM, Nancollas GH. Tracking Amorphous Precursor Formation and Transformation during Induction Stages of Nucleation. *Cryst Growth Des.* 2014;14(4):1659–65.
  62. Paul H, Reginato AJ, Schumacher HR. Alizarin red S staining as a screening test to detect calcium compounds in synovial fluid. *Arthritis rheumatism.* 1983;26(2):191–200.
  63. Puchtler H, Meloan SN, Terry MS, On the history and mechanism of alizarin and alizarin red S stains for calcium. *J Histochem Cytochem.* 1969;17(2):110–24.
  64. Stanford CM, Jacobson PA, Eanes ED, Lembke LA, Midura RJ. Rapidly forming apatitic mineral in an osteoblastic cell line (UMR 106-01 BSP). *J Biol Chem.* 1995;270(16):9420–8.
  65. Simon P, Grüner D, Worch H, Pompe W, Lichte H, El Khassawna T, Heiss C, Wenisch S, Kniep R. First evidence of octacalcium phosphate@osteocalcin nanocomplex as skeletal bone component directing collagen triple-helix nanofibril mineralization. *Sci Rep.* 2018;8(1):13696.
  66. Figueiredo MM, Gamelas J, Martins G. Characterization of bone and bone-based graft materials using FTIR spectroscopy, 2012.
  67. Paschalis EP, Mendelsohn R, Boskey AL. Infrared assessment of bone quality: a review. *Clin Orthop Relat Res.* 2011;469(8):2170–8.
  68. Boskey AL, Roy R. Cell culture systems for studies of bone and tooth mineralization. *Chem Rev.* 2008;108(11):4716–33.
  69. Phillips JE, Hutmacher DW, Guldberg RE, Garcia AJ. Mineralization capacity of Runx2/Cbfa1-genetically engineered fibroblasts is scaffold dependent. *Biomaterials.* 2006;27(32):5535–45.
  70. Kumar A, Young C, Farina J, Witzl A, Marks ED. Novel nanocomposite biomaterial to differentiate bone marrow mesenchymal stem cells to the osteogenic lineage for bone restoration. *J Orthop Transl.* 2015;3(3):105–13.
  71. Addison WN, Nelea V, Chicatun F, Chien YC, Tran-Khanh N, Buschmann MD, Nazhat SN, Kaartinen MT, Vali H, Tecklenburg MM, Franceschi RT, McKee MD. Extracellular matrix mineralization in murine MC3T3-E1 osteoblast cultures: an ultrastructural, compositional and comparative analysis with mouse bone. *Bone.* 2015;71:244–56.

**Publisher's Note** Springer Nature remains neutral with regard to jurisdictional claims in published maps and institutional affiliations.